LAWRENCE
LIVERMORE
NATIONAL
LABORATORY

UCRL-JRNL-225679

Aerosol sample preparation methods for X-ray diffractive imaging: Size-selected spherical nanoparticles on silicon nitride foils

M. J. Bogan, W. H. Benner, S. Hau-Riege, H. Chapman, M. Frank

October 30, 2006

Journal of Aerosol Science

Updated October 14, 2003

Aerosol sample preparation methods for x-ray diffractive imaging: Size-selected spherical nanoparticles on silicon nitride foils

Michael J. Bogan, W. Henry Benner, Stefan P. Hau-Riege, Henry N. Chapman, Matthias Frank*

Lawrence Livermore National Laboratory, 7000 East Avenue, Livermore, California 94550

Author email address: bogan2@llnl.gov

Title running head: X-ray scattering of size-selected nanoparticles

*Corresponding author: Michael J. Bogan, Medical Physics and Biophysics Division, Physics and Advanced Technologies Directorate, Lawrence Livermore National Laboratory, 7000 East Ave. Livermore, CA 94550 phone: 1-925-423-5920 fax: 1-925-424-2778 email: bogan2@llnl.gov

ABSTRACT We are developing aerosol generation and processing methods for x-ray analyses of nanoscale materials using conventional synchrotron radiation sources and using the newly operational soft x-ray free-electron laser in Hamburg (FLASH) at the Deutsches Elektronen Synchrotron. Charge-reduced electrospray, differential mobility analysis and an electrostatic precipitator were used to prepare samples consisting of size-monodisperse spherical nanoparticles deposited on 20 nm thick silicon nitride foils supported by silicon frames. 97 and 102 nm diameter spheres were selected from a broader distribution of 98 nm spheres using differential mobility. We measured the size distribution of the spheres using forward scattering from 1.65 nm light at the Advanced Light Source (ALS) in Lawrence Berkeley National Laboratory and scanning electron microscopy (SEM). The full-width half maximum (FWHM) of the size-distribution of the size-selected spheres was as narrow as 5.4 nm when measured by SEM, as compared to 16 nm for the non-size-selected distribution. Forward scattering measurements of the 97 nm diameter size-selected spheres fit a size distribution with a FWHM of 4 nm and allowed us to validate the methodology for use in future diffraction imaging experiments at FLASH.

Keywords: electrospray, differential mobility, nanoparticle, x-ray diffractive imaging

1. Introduction

Scattering of ultraviolet (UV) or visible light, as described by Mie theory, is a standard approach for characterizing the properties of spherical particles (van de Hulst, 1981). Angle-resolved measurements of the scattered light intensity provide a way to calculate particle size and index of refraction. The primary goal of this study is to validate the use of aerosol methods for preparation of size-monodisperse spherical nanoparticles that will be used as targets in future experiments designed to study laser-matter interaction at the world's first free electron laser functioning in the soft x-ray regime, the free electron laser in Hamburg (FLASH). One of the goals of the FLASH experiments is to determine the change of particle properties (size and refractive index) from the diffraction pattern recorded from single x-ray pulses, as a function of pulse fluence. This will enable us to study the response of materials, on a submicron length scale, as they are rapidly heated to hot (60000 K) dense plasma (Chapman *et al.*,

2006) by the FLASH pulses. That is, the scattering pattern from the single pulse will be used to examine the effect of that pulse on the material over the pulse duration. With lower fluence non-damaging pulses, these types of samples will also be useful for studying ultrafast dynamics of materials (for example, near phase transitions). Spherical nanoparticles offer both modeling and experimental advantages as test objects because interpretation of their diffraction patterns is well understood. A spread in the initial diameters of the spheres causes line broadening in the diffraction pattern that reduces the resolution of the measurement of changes in particle size and optical properties. These measurements therefore require samples prepared with size-monodisperse spheres to optimize the resolution. Furthermore, signal levels in FLASH experiments will depend on the magnitude of the photon fluence and the number of spheres irradiated. Thus a protocol for creating samples with different numbers of spheres (estimated to be 1-1000 particles per FLASH pulse, corresponding to a range of $3x10^{-3}$ to 3 particles/μm^2) is required.

We addressed these requirements by preparing size-monodisperse spherical nanoparticle samples using electrospray differential mobility size-selection and electrostatic deposition (Fissan *et al.*, 2003). Polystyrene spheres ~100 nm in diameter are deposited onto silicon nitride (Si_3N_4) foils (Anastasi & Burge, 1990) that are thinner than the sphere diameter and transmissive to x-rays, thus facilitating diffraction imaging experiments. Diffraction imaging is elegant in its experimental simplicity: a coherent X-ray beam illuminates the sample and the far-field diffraction pattern of the object is recorded on an area detector (in this case a bare CCD chip). In this work, x-rays scattered from particles positioned on the foil are transmitted through the 20 nm thick Si_3N_4 foil and are detected by a CCD camera (Figure 1). The x-ray scattering data collected with conventional synchrotron radiation serves as a proof-of-concept for this sample preparation methodology for future FLASH diffraction imaging experiments.

Under its initial operating parameters, FLASH emits intense 25 fs, 4 x 10^{13} W/cm^2 pulses containing 10^{12} photons at 32 nm wavelength. Interaction of a single pulse with a nano-structured non-periodic object produces a coherent diffraction pattern that can be recorded using specially designed x-ray optics and a CCD. An iterative algorithm, Shrinkwrap (Marchesini *et al.*, 2003), uses the information in the

diffraction pattern to reconstruct the image of the object irradiated by the single pulse. The first demonstration of this experiment, femtosecond diffractive imaging (Chapman *et al.*, 2006), confirmed predictions (Bergh *et al.*, 2004; Hau-Riege *et al.*, 2004; Jurek *et al.*, 2004; Neutze *et al.*, 2000) that the diffraction pattern created from a non-crystalline object irradiated by such a pulse would be representative of the structure of the object before the manifestation of damage. The spherical nanoparticle samples prepared and characterized here will be used as targets for x-ray pump-probe measurements using the ultrafast laser pulses that will enable us to measure the dynamics of the explosion on very short time scales.

2. Experimental

2.1 Nanoparticle Aerosolization and Deposition

The nanoparticles used in this work are polystyrene spheres (PostNova, Germany) with a reported diameter of 98 nm and a coefficient of variance of 5.4 %. They are provided in a surfactant-free solution at a concentration of 1.5×10^{14} particles/ml (p/ml). Solutions that contain surfactants to stabilize the spheres were also studied but solution-viscosity modifications due to the surfactant destabilized the electrospray process used to aerosolize the spheres. When solutions containing surfactants are electrosprayed, particles <10 nm in diameter are detected in addition to the spheres. These particles are the residues of droplets that contain no spheres. The formation of these residue particles suggests that electrospraying solutions of spheres that also contain surfactants results in spheres coated by surfactants (Kaufman, 2000). To eliminate the potential for coated spheres, only surfactant-free spherical nanoparticle solutions are used to prepare samples for x-ray studies.

To characterize the sphere size distribution and to reduce their size-polydispersity we use charge-reduced electrospray and differential mobility analysis technology (Lenggoro *et al.*, 2002). Figure 2A describes the apparatus and procedure for collecting size-selected spheres onto Si_3N_4 foils. An electrospray aerosol generator (TSI model 3480) is used to aerosolize solutions of 1.5×10^{12} to 1.5×10^{13} p/ml prepared in 25 mM ammonium acetate in water. Similar to previous studies (Bacher *et al.*, 2001; Chen *et al.*, 1995) 25-100 μL of sample in a 1.5 ml plastic microcentrifuge tube is placed in the

cylindrical pressure chamber of the electrospray generator. A capillary of 40 μm inner diameter and a platinum wire at a voltage of 2.0 kV make contact with the sample. A differential pressure of 1.2 psi forces the solution through the capillary at about 0.1 uL/min. The voltage applied to the sample creates a Taylor cone at the tipped exit of the capillary. These electrospray conditions produce primary droplets 150 nm to 200 nm in diameter. (Chen *et al.*, 1995)

The electrospray droplets are introduced into a flow of 1.5 lpm air and 0.1 lpm CO_2 to minimize corona discharge. The droplets are immediately charge-reduced by exposure to ionized air created by a ^{210}Po α-source and allowed to evaporate to dryness, resulting in an aerosol of discrete aerosolized spheres with a known charge distribution. The charge carried by the spheres is predominantly zero, while a small fraction is singly-charged (positively or negatively), and an even smaller fraction is doubly-charged (again, positively or negatively), as predicted by Fuchs' particle charge distribution (Fuchs, 1963; Hoppel & Frick, 1986), also called a Boltzman charge distribution (Liu & Pui, 1974). The size-polydisperse spheres pass into a differential mobility analyzer (DMA) (TSI, model 3081) via a conductive silicone tube and are size-classified based on their electrical mobility. A portion of the size-selected aerosol is sampled into a condensation particle counter (CPC) (TSI, model 3786) to monitor the gas phase particle concentration (number/cm^3) and the remaining aerosol is delivered to a nanometer aerosol sampler (NAS) (TSI, model 3089) for electrostatic capture onto a substrate (Dixkens & Fissan, 1999). Silicon wafers (1 cm^2) supporting the Si_3N_4 foils are positioned with electrically conductive tape onto a 1 cm diameter electrode (-10 kV) in the NAS. The particle size distribution was measured by scanning the DMA electrode voltage while counting the particles entering the CPC. The DMA data was not corrected for the finite width response of the DMA.

During sample preparation, aerosol concentration (*C*) of size-selected spheres indicated by the CPC is used as a real-time diagnostic of the stability of the electrospray conversion of the spheres in solution to an aerosol. From *C,* the total number of spheres that enters the NAS for collection on the foil, (*N*), is calculated using the relationship N = *Cft*, where *f* is the flow rate of the gas carrying the aerosol into the NAS and *t* is the total exposure time. N is used to provide an estimate of the number of spheres on the

surface of the sample. SEM is used to measure the actual number of spheres on the foil. The total number of spheres in an area of 20 μm^2 is counted in 5-10 images to provide an average number of spheres/μm^2 on the surface.

Figure 2B describes the method used to coat a single sample with different densities of spherical nanoparticles by exposing discrete regions of the sample to a different absolute number of spheres. In this example, a sample with four regions is created. The number of regions that can be made on a sample surface can be increased or decreased to fit experimental requirements. In step 1, a mask is used to cover a portion of the foil. The uncovered area is exposed to a known number of spheres N_1. The spheres are electrostatically deposited on the sample to a resultant coverage of D (spheres/μm^2). In step 2, the mask is moved so that a larger region, that includes the first region, is exposed to another known number of spheres N_2. Thus two regions are created, the first is exposed to $N_1 + N_2$ spheres and the second to N_2 spheres. Continuing in this manner for n steps produces n discrete regions on the foil with decreasing exposures of spheres as n increases, i.e. $D_1 > D_2 > \ldots D_n$.

2.2 X-ray analysis

The thin foils (thickness less than the radius of the spheres) are designed to cause minimal interference from x-rays scattered from the foil. The foils are prepared on 300 μm thick Si wafers following the procedure of (Anastasi & Burge, 1990). The basic procedure starts by coating both sides of a standard Si wafer with Si_3N_4. One side of the wafer is then coated with photoresist, masked and exposed to UV light. Si_3N_4 in areas once covered by photoresist is removed by hydrofluoric acid etching or plasma etching. Uncovered Si is removed by potassium hydroxide anisotropic etch to leave free standing Si_3N_4 foils. Foils can be created with a large variation in dimensions but for experiments reported here they are 20 nm thick and 1750 μm x 50 μm. A thickness of 20 nm is chosen because it represents a functional balance between high x-ray transmission, fabrication ease, and operational integrity. The transmission of a 20 nm thick foil at a wavelength of 1.65 nm is 97 %. Si-supported Si_3N_4 foils are also commercially available (SPI Supplies Structure and Probe Inc., PA).

X-ray scattering experiments were performed at beamline 9.0.1 at the ALS. The experimental vacuum chamber in which the experiments were performed has been described in detail (Beetz *et al.*, 2004; Howells *et al.*, 2002). An off-axis zone-plate monochromator is used to select the third harmonic of a 10-cm-period undulator beamline. The 1.65 nm light is passed through a 5 μm pinhole and diverges to illuminate about a 10 μm diameter spot on the sample with a flux of ~10^9 photons s^{-1} um^{-2} (Figure 1). An in-vacuum backside illuminated CCD camera (MTE-2, Roper Scientific, Inc) with a 1340x1300 array of 20 μm square pixels is used to capture the scattering signal at a position 11.8 cm from the sample. This enables detection of scattering light over an angular range of about 7° on either side of the optical axis. A translatable opaque beamstop prevents saturation and radiation damage of the center CCD pixels while collecting the higher angle scatter. Individual samples are translated into the beam using motion controllers, until the foil supporting the spheres is illuminated and then the scatter signal is optimized. CCD integration time is 3-20 minutes. Background corrected data was compared to Mie theory using a refractive index of 0.9956411 with an imaginary component of 6.1915517×10^{-5}.

3. Results and Discussion

3.1 Size-monodisperse spherical nanoparticles on Si_3N_4 foils

The size distribution of the 98 nm polystyrene spheres obtained from PostNova was measured using a DMA (Figure 3A). A Gaussian fit of this data shows the most abundant diameter of the particles by percent concentration is 99.9±0.2 nm, and the full width at half maximum (FWHM) of the distribution is 16 nm. While the SEM measurement of the particle size distribution (Figure 3B) agreed with the DMA measurement, the manufacturer's reported FWHM is 12.5 nm, assuming a normal distribution. Nonetheless, the width of this size distribution is too large for future FLASH experiments because this width will broaden (smear) the sphere diffraction patterns. We want to demonstrate that in future experiments at FLASH we will be able to measure changes in sphere diameter as small as a 5 % expansion, while a particle explodes. To do so we need starting distributions to be as narrow as possible.

We used commercially available aerosol processing technology to size-select spherical nanoparticles, reducing the polydispersity to an acceptable level.

To demonstrate the sample preparation method and x-ray scattering measurements, an example of two samples that were prepared with size-selected spherical nanoparticles collected onto foils with up to 3.2 nanoparticles/μm^2 will be used. The stock solution of 98 nm diameter spheres was electrosprayed and the DMA was set to transmit a specific diameter by changing the voltage applied to the DMA (-2465.3 V and -2704.9 V for 97 and 102 nm diameter spheres, respectively). Comparison of SEM images of spheres from the polydisperse source aerosol and spheres size-selected from the same aerosol illustrates the capability of the DMA to transmit a narrow size distribution of spheres (Figure 4). For example, in a randomly selected foil coated with non-size-selected spheres, four adjacent spheres had nominal diameters of 73, 80, 93, and 100 nm (Figure 4A) whereas six adjacent spheres on the sample prepared with size-selection all had measured diameters of 97 nm (Figure 4B). Other key features revealed in these micrographs are the local uniformity of the Si_3N_4 foil and the absence of contaminant particulate matter. All material irradiated by the x-ray beam contribute to the diffraction image so clean surfaces are essential for generating high quality images.

The diameters of >200 spheres for both sizes selected were also measured by SEM. Histograms of the size-selected sphere diameters (Figure 3C) show the efficacy of DMA size-selection when compared with the non-size-selected population in Figure 3B. For comparison, the size-selected histogram data were converted into percent concentration and Gaussian fits were overlayed onto Figure 3A. The FWHM of these fits were 5.4 and 6.5 nm for the 97 and 102 nm diameter particles, respectively. This data provides a clear representation of the improved monodispersity due to DMA particle size-selection under these conditions from the original size distribution with a FWHM >10 nm.

SEM images were also used to determine the extent of coverage of nanoparticles on the Si_3N_4 foil. In this example, a single image of each of the four discrete regions was taken at equal magnification. The four regions contained 86, 39, 10, and 3 spheres, respectively (Figure 4 C-F), confirming that the mask procedure did result in $D_1 > D_2 > D_3 > D_4$ (refer to Figure 2B). For measurements made from additional samples prepared over a period of weeks, D was found to correlate linearly with N ($R^2 = 0.97$). The

resulting relationship, $D = (-0.03\pm0.04) + (6.5\pm0.04)\text{x}10^{-9}(N)$, was used to determine an estimate of D in real time, eliminating unnecessary and timely measurements of D by SEM during preparation of samples with a specific desired number of spheres on the surface. The time required to prepare a sample varies from 5 to 600 minutes or higher depending on the desired D and the aerosol concentration.

In all images analyzed, greater than 98.5 % of 97 nm spheres occupied distinct positions on the Si_3N_4 foils. The remaining 1.5 % existed as pairs in contact. Very rare instances of 3 spheres contacting were observed. If the sphere deposition followed Poisson statistics, a higher occurrence of pairs in contact is expected. This deviation is likely due in part to the repulsion forces present from the like charges on the spheres. Distinct positioning of the nanoparticles is a desirable characteristic of the sample preparation because the x-ray penetration depth into polystyrene is about 15 μm so a pile of ~150 spheres would distort the scatter signal observed. In the areas analyzed to prepare the histogram of non-size selected spheres diameters, several clusters of spheres ~1 μm in diameter and 1 cluster of ~8 μm were observed. These large aggregates are much larger than the droplet size produced by the stable mode of electrospray thus were likely formed during an unstable pulsing mode of the electrospray process. Preparation of samples using DMA size-selection has no risk of such aggregates existing on a sample and only at unreasonably long deposition times could a layer of spheres thicker than the penetration depth be formed. By contrast, the aggregation resulting from direct deposition from solution is much more likely to result in localized nanoparticle aggregates thicker than the x-ray penetration depth.

3.2 X-ray measurement of DMA size-selected spherical nanoparticles

Scatter signal was integrated for 21 and 11 minutes for 97 and 102 nm diameter spheres, respectively (Figure 5A and 5B). It is estimated that three hundred spheres occupied the area irradiated by the x-ray beam, providing sufficient the signal-to-noise ratio of the scattering intensity while retaining a diffraction pattern consistent with that of a single sphere. Furthermore, the Si_3N_4 foil preparation method produces sufficiently thin and clean substrates as to not interfere with the sphere diffraction. A plot of the radial average of the CCD signal as a function of angle (radial pixel position) facilitates visualization of the change in the minima of the diffraction pattern due to particle diameter change

(Figure 5C). Minima for the 102 nm diameter spheres are at smaller angles than minima for the smaller spheres (2.30 and 2.37 for the 3rd minimum, respectively – see inset Figure 5C), thus the particles were prepared with sufficient monodispersity to differentiate a 5 nm change in diameter using the diffraction patterns. Seven minima are observed in the radial averages, suggesting the population of spheres measured is highly size monodisperse.

Mie theory was used to determine the size distribution of spheres that best fit our experimental results. Summarized in Figure 6, this analysis showed that distributions with a FWHM of 10 nm clearly resolved too few minima and thus DMA size-selection increased monodispersity to less than 10 nm FWHM. The best fit for our data was a FWHM between of 4 nm (inset Figure 6). This measurement is in general agreement with the SEM data, further supporting the usefulness in these experiments of the size-selection capability of the DMA. Background scattering from the Si_3N_4 foil was a variable in our measurement and may account for the difference with the SEM. A more accurate measurement of the size distribution with more rigorous background corrections is possible. Nonetheless, the reduction in size-polydispersity of the aerosol imparted by DMA size selection has been validated by SEM and x-ray scattering measurements of samples that can be used as targets for future FLASH experiments.

4. Discussion

Both the SEM and x-ray measurements presented here confirm that samples consisting of a population of ~100 nm diameter spherical nanoparticles with FWHM <5 nm can be prepared on Si_3N_4 foils. Note that the methodology is not limited to the sphere sizes in the example reported here. Spherical nanoparticles of 88 and 140 nm in diameter have also been size-selected with similar results (data not shown). Furthermore, the method is applicable to any nanoscale biomaterials, such as viruses, amenable to electrospraying (Hogan, 2006). Samples created using this method will act as standards for the characterization of FLASH pulse interaction with matter in pump-probe experiments and for femtosecond diffractive imaging of nanoparticles. The ALS x-ray scattering measurements reported here can differentiate between the two diameters of size-selected nanoparticles with a 5 nm difference verified by scanning electron microscopy. Thus, in future FLASH experiments it will be possible to detect similar changes in sphere diameter due to any explosion. In short, we have used the

measurements on two sets of size-selected spheres to mimic a diameter change due to an explosion that may be measured at FLASH in the future. During such experiments the 20 nm thick Si_3N_4 foil will transmit at only 42 % instead of 97 % because of the change in wavelength from 1.65 nm to 32 nm. Future upgrades of FLASH to 13 and 6 nm will allow transmission of 75-85 %. The ability to control the number of spheres positioned on the Si_3N_4 foils, as demonstrated here, will be critical to preparation of samples to meet these changing criteria.

New methods for controlled delivery of free nanoparticles to x-ray free-electron-lasers must also be developed to remove substrate effects from the x-ray measurements of individual nanoparticles. Thus, future work will also include adaptation of the method for injection of free nanoparticles to the FLASH pulses. In this approach, the size-selected nanoparticles will be delivered into a differentially pumped aerodynamic focusing system that will generate a beam of nanoparticles that can be steered into the FLASH pulses. The successful characterization of nanoparticles using the new intense x-ray sources such as FLASH and the Linac Coherent Light Source at the Stanford Linear Accelerator Center will rely heavily on adaptations of existing aerosol sample preparation methods such as those described here.

5. Conclusions

Aerosol methods for preparing size-monodisperse spherical nanoparticles as fixed target standards for x-ray diffractive imaging were validated using conventional synchrotron radiation and SEM. The number of spheres in a specific area of a Si_3N_4 foil can be controlled and essentially all of the spheres occupy distinct positions, ensuring the integrity of the diffraction pattern recorded. SEM and x-ray scattering measurements showed that DMA filtered polystyrene particles have size distributions adequately narrow (FWHM ~5 nm at ~100 nm diameter) to produce high quality scattering images. This aerosol method will be used to prepare samples for femtosecond diffractive x-ray imaging of nanoparticles using x-ray free-electron lasers.

Acknowledgements

The authors thank David Shapiro and Stefano Marchesini for technical assistance with ALS experiments & Sebastien Boutet and the reviewers for comments on the manuscript. This work was supported by the following agencies: The U.S. Department of Energy under Contract W-7405-Eng-48 to the University of California, Lawrence Livermore National Laboratory; Project 05-SI-003 from the Laboratory Directed Research and Development Program of LLNL; and The National Center for Electron Microscopy and the Advanced Light Source, Lawrence Berkeley Lab, under DOE Contract DE-AC02-05CH11231. UCRL-JRNL-225679. M. Bogan is a Natural Sciences and Engineering Research Council of Canada (NSERC) Postdoctoral Fellow.

References

Anastasi, P.A.F. and Burge, R.E. (1990) Preparation and characterization of silicon nitride membranes for soft X-ray microscopy. In *X-ray Microscopy III* (Edited by Michette A. G., Morrison G. R. and Buckley C. J.), Springer-Verlag, London.

Bacher, G., Szymanski, W.W., Kaufman, S.L., Zollner, P., Blaas, D. and Allmaier, G. (2001) Charge-reduced nano electrospray ionization combined with differential mobility ananlysis of peptides, proteins, glycoproteins, noncovalent protein complexes and viruses *Journal of Mass Spectrometry* **36**, 1038-1052.

Beetz, T., Howells, M.R., Jacobsen, C., Kao, C.-C., Kirz, J., Lima, E., Mentes, T.O., Miao, H., Sanchez-Hanke, C., Sayre, D. and Shapiro, D. (2004) Apparatus for X-ray diffraction microscopy and tomography of cryo specimens *Nuclear Instruments and Methods A* **545**, 459-468.

Bergh, M., Timneanu, N.O. and van der Spoel, D. (2004) Model for the dynamics of a water cluster in an x-ray free electron laser beam *Physical Review E* **70**, 051904.

Chapman, H.N., Barty, A., Bogan, M.J., Boutet, S., Frank, M., Hau-Riege, S.P., Marchesini, S., Woods, B.W., Bajt, S., Benner, W.H., London, R.A., Plonjes, E., Kuhlmann, M., Treusch, R., Dusterer, S., Tschentscher, T., Schneider, J.R., Spiller, E., Moller, T., Bostedt, C., Hoener, M., Shapiro, D.A., Hodgson, K.O., van der Spoel, D., Burmeister, F., Bergh, M., Caleman, C., Huldt, G., Seibert, M.M., Maia, F.R.N.C., Lee, R.W., Szoke, A., Timneanu, N. and Hajdu, J. (2006) Femtosecond diffractive imaging with a soft-X-ray free-electron laser *Nature Physics* **2**, 839-843.

Chen, D.R., Pui, D.Y.H. and Kaufman, S.L. (1995) Electrospraying of conducting liquids for monodisperse aerosol generation in the 4 nm to 1.8 um diameter range *Journal of Aerosol Science* **26**, 963-977.

Dixkens, J. and Fissan, H. (1999) Development of an electrostatic precipitator for off-line particle analysis *Aerosol Science and Technology* **30**, 438-453.

Fissan, H., Kennedy, M.K., Krinke, T.J. and Kruis, F.E. (2003) Nanoparticles from the gas phase as building blocks for electrical devices *Journal of Nanoparticle Research* **5**, 299-310.

Fuchs, N.A. (1963) On the stationary charge distribution on aerosol particles in a bipolar ionic atmosphere *Geophysica pura e applicata* **56**, 185-193.

Hau-Riege, S.P., London, R.A. and Szoke, A. (2004) Dynamics of x-ray irradiated biological molecules *Physical Review E* **69**, 051906.

Hogan, C.J.J., Kettleson, E.M., Ramaswami, B., Chen, D.R., Biswas, P. (2006) Charge reduced electrospray size spectrometry of mega- and gigadalton complexes: whole viruses and fragments *Analytical Chemistry* **78**, 844.
Hoppel, W.A. and Frick, G.M. (1986) Ion attachment coefficients and the steady state charge distribution on aerosols in a bipolar environment *Aerosol Science and Technology* **5**, 2-21
Howells M.R., Charalambou, P., He, H., Marchesini, S. and Spence, J.C.H. (2002) Off-axis zone plate monochromator for high-power undulator radiation *SPIE: Design and microfabrication of novel x-ray optics, Seattle, WA.*
Jurek, Z., Faigel, G. and Tegze, M. (2004) Dynamics in a cluster under the influence of intense femtosecond hard x-ray pulses *European Journal of Physics D.* **29**, 217-229.
Kaufman, S.L. (2000) Electrospray diagnostics performed by using sucrose and proteins in the gas-phase electrophoretic mobility molecular analyzer (GEMMA) *Analytica Chimica Acta* **406**, 3-10.
Lenggoro, I.W., Xia, B., Okuyama, K. and Fernandez de la Mora, J. (2002) Sizing of colloidal nanoparticles by electrospray and differential mobility analyzer methods *Langmuir* **18**, 4584-4591.
Liu, B.Y.H. and Pui, D.Y.H. (1974) Equilibrium bipolar charge distribution of aerosols *Journal of Colloid and Interface Science* **49**, 305-312.
Marchesini, S., He, H., Chapman, H.N., Hau-Riege, S.P., Noy, A., Howells, M.R., Weierstall, U. and Spence, J.C.H. (2003) X-ray image reconstruction from a diffraction pattern alone *Physical Review B* **68**, 140101(R).
Neutze, R., Wouts, R., van der Spoel, D., Weckert, E. and Hajdu, J. (2000) Potential for biomolecular imaging with femtosecond x-rays *Nature* **406**, 752-757.
van de Hulst, H.C. (1981) Light scattering by small particles New York Dover Publications, Inc.

Figure Captions

Figure 1. X-ray diffraction experiment at ALS. The sample of spherical nanoparticles positioned on a Si_3N_4 foil (A) supported in a silicon frame (B), is positioned into the pulsed x-ray beam (C). The resultant diffraction pattern (D) is recorded using a CCD camera (E) and the direct beam is stopped by a beamstop (F). The silicon chip is depicted as a cross-section to reveal the thickness of the foil (20 nm) relative to the chip (300 μm thick). This figure is not drawn to scale.

Figure 2. A) Instrumental setup for aerosolization, size-selection, and collection of spheres on Si_3N_4 foils. **B)** Strategy for varying the exposure time (t) to different areas of the foil to control sphere coverage (D) on the surface.

Figure 3. (A) Size distribution of the electrosprayed stock solution of 98 nm polystyrene spheres as measured using differential mobility analysis. The dotted line is a Gaussian fit (FWHM = 16 nm) to the DMA data (filled squares). The red and green traces are Gaussian fits to SEM data obtained when the

DMA was set to transmit 97 (red) and 102 (green) diameter spheres. (B) Histogram of SEM diameter measurements of 299 non-size-selected spheres (before DMA filtering). (C) Histograms of SEM diameter measurements of 237 DMA size-selected 97 nm spheres (open red bars) and 231 102 nm size-selected spheres (solid green bars) used to create traces in (A). Sphere diameters were separated into 1 nm bins for all histograms.

Figure 4. Scanning electron micrographs of spherical nanoparticles **(A)** without size-selection and **(B)** with the DMA set to transmit 97 nm diameter particles. Scale bars are 100 nm long. Wider field micrographs of a single foil with four regions exposed to decreasing numbers of 97 nm diameter particles: **(C)** D_1=1.10, **(D)** D_2=0.45, **(E)** D_3=0.11, and **(F)** D_4=0.02 particles/μm^2. The scale bar in (C) represents 2 μm. Image contrast and brightness was modified to enhance visualization of the particles.

Figure 5. CCD images of forward scattered 1.65 nm radiation from **A)** 102 nm diameter particles at 3.2 particles/μm^2 and **B)** 97 nm diameter spheres at 3.2 particles/μm^2 positioned on 20 nm thick Si_3N_4 foils. The black area represents an area removed from radial average calculations because it either contained scatter from the edges of the foil or contained no signal due to the beam stop. **(C)** Radial averages of the angle-resolved scatter signal for 102 nm diameter (green) and 97 nm diameter (red) spheres. Dotted lines show angle-resolved scatter intensity after background correction. The inset highlights the change in angle of the 2nd minimum due to a 5 nm difference in sphere diameter.

Figure 6. Comparison of experimental diffraction results for the 97 nm diameter spheres (solid blue line) with Mie theory calculated for a distribution of spheres with FWHM of 3, 4, 5, 10 nm (green, red, black, and grey dotted lines, respectively). The inset is a closeup of the third minimum, showing that the intensity at the minimum fits best to Mie calculations based on a 4 nm FWHM particle size distribution.

Figures

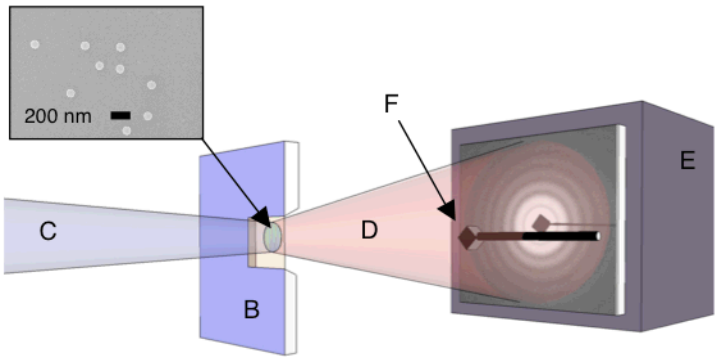
200 nm
F
E
C
D
B

Figure 1

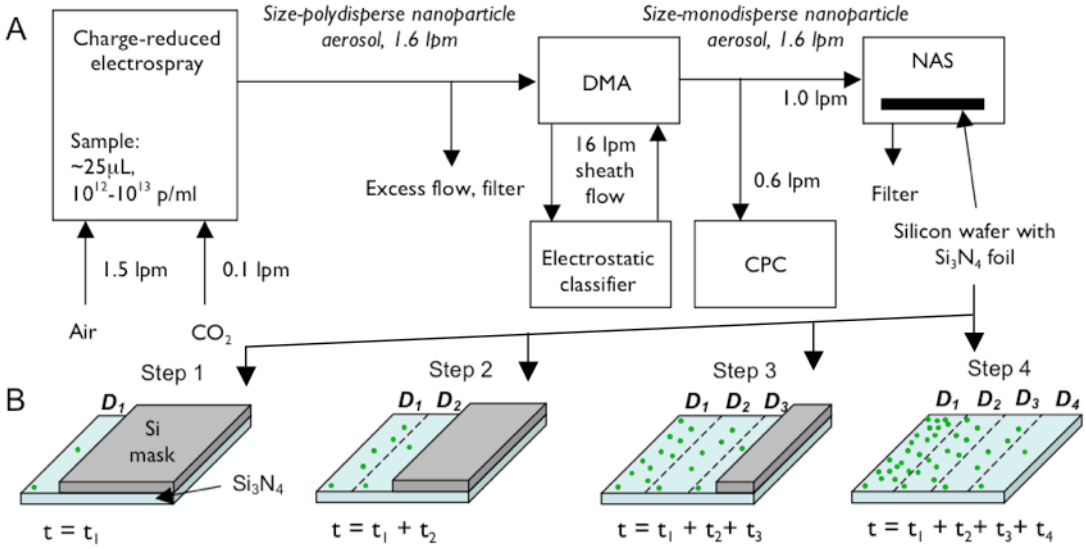
A
Charge-reduced electrospray
Sample:
~25μL,
10^12-10^13 p/ml
Size-polydisperse nanoparticle aerosol, 1.6 lpm
DMA
Size-monodisperse nanoparticle aerosol, 1.6 lpm
NAS
1.0 lpm
Excess flow, filter
16 lpm sheath flow
0.6 lpm
Filter
Silicon wafer with Si3N4 foil
Electrostatic classifier
CPC
1.5 lpm
0.1 lpm
Air
CO2
B
Step 1
Step 2
Step 3
Step 4
D1
D2
D3
D4
Si mask
Si3N4
t = t1
t = t1 + t2
t = t1 + t2+ t3
t = t1 + t2+ t3+ t4

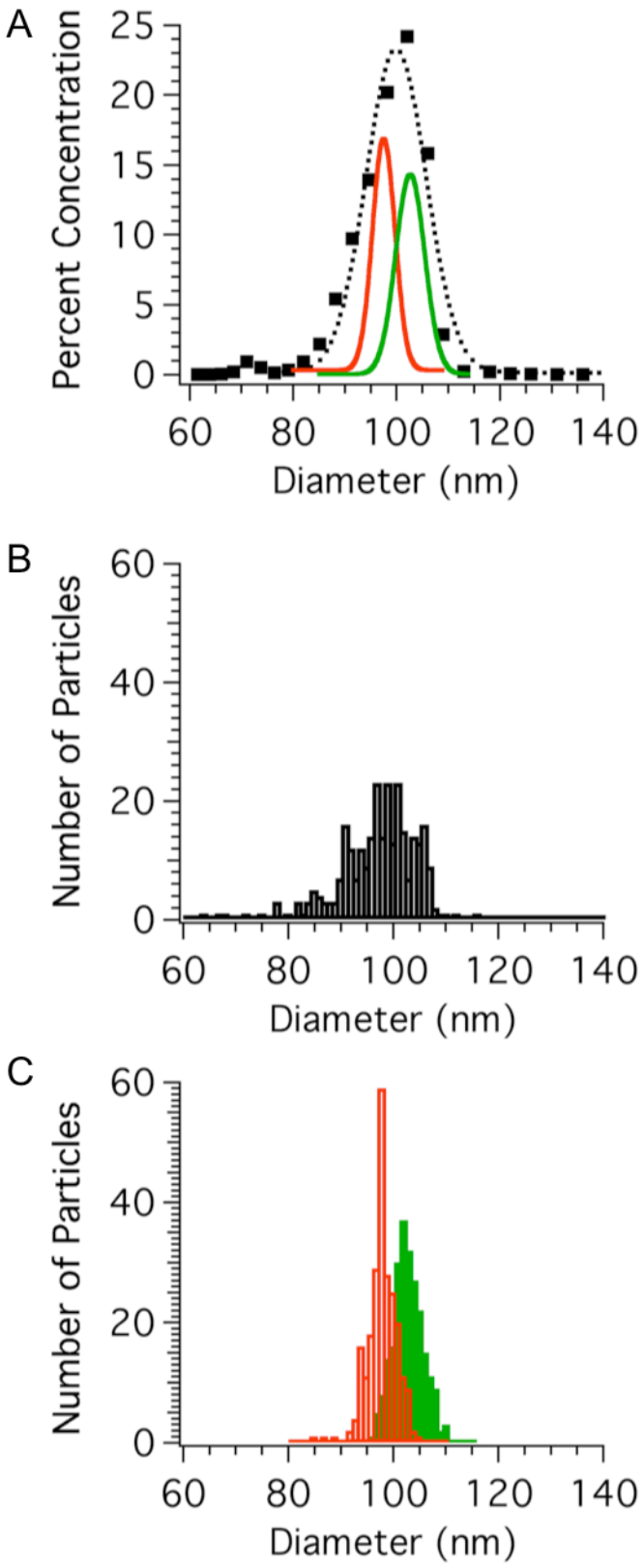
A
Percent Concentration
25
20
15
10
5
0
60
80
100
120
140
Diameter (nm)
B
Number of Particles
60
40
20
0
60
80
100
120
140
Diameter (nm)
C
Number of Particles
60
40
20
0
60
80
100
120
140
Diameter (nm)

Figure 3

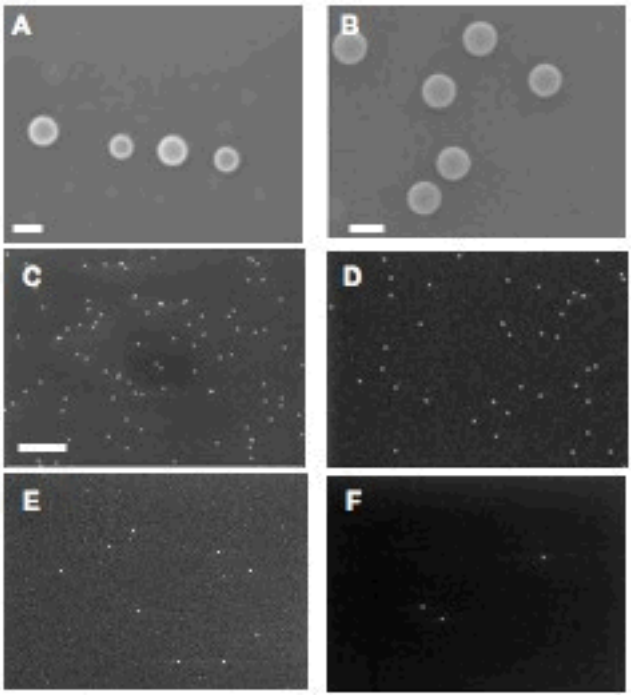

Figure 4

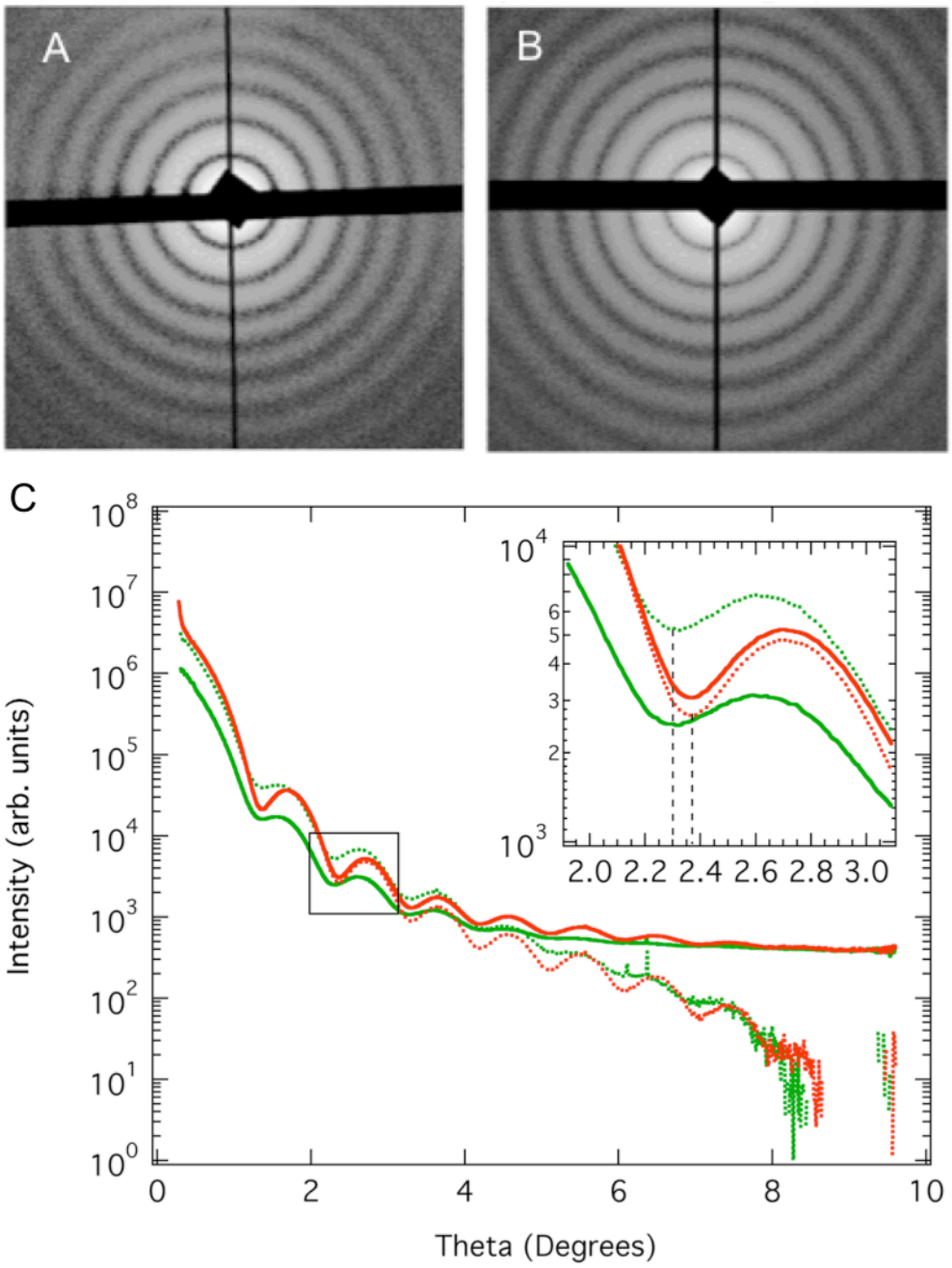
A
B
C
Intensity (arb. units)
Theta (Degrees)
10^0
10^1
10^2
10^3
10^4
10^5
10^6
10^7
10^8
0
2
4
6
8
10
10^4
6
5
4
3
2
10^3
2.0 2.2 2.4 2.6 2.8 3.0

Figure 5

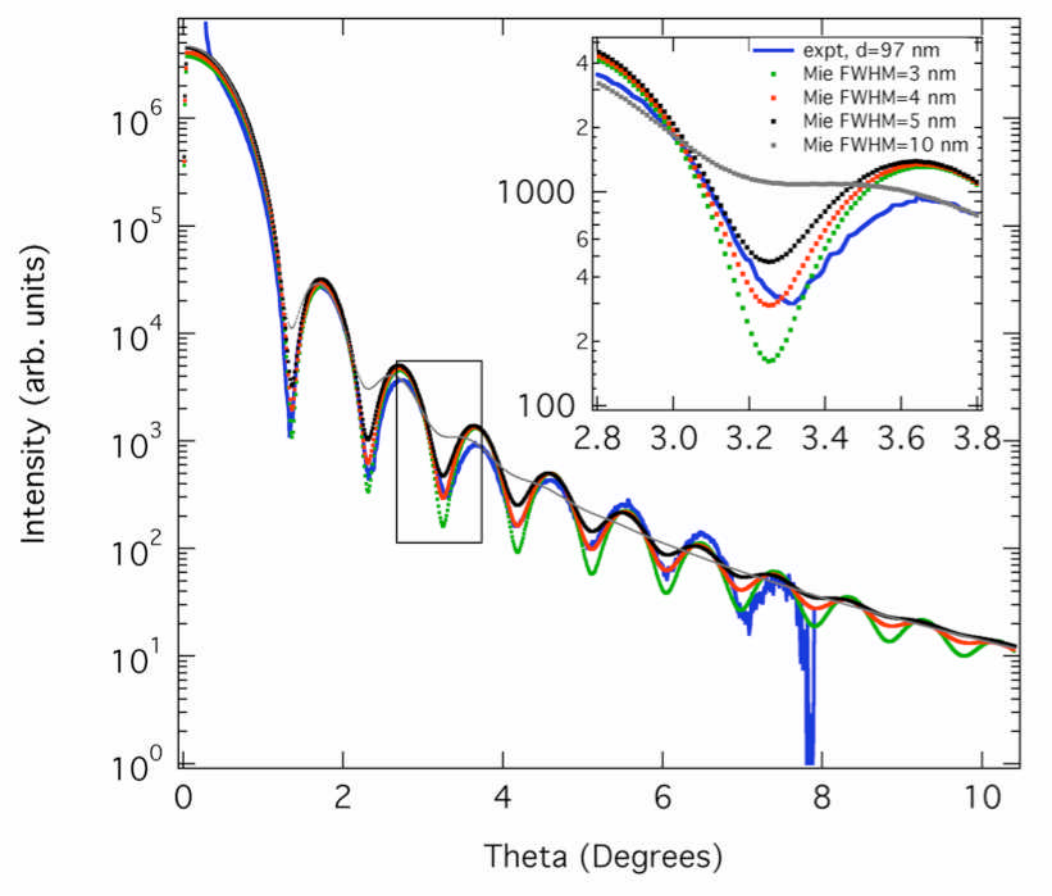
Intensity (arb. units)
Theta (Degrees)
expt, d=97 nm
Mie FWHM=3 nm
Mie FWHM=4 nm
Mie FWHM=5 nm
Mie FWHM=10 nm

Figure 6